



Cite this: *Nanoscale*, 2016, 8, 12579

## Detection of early primary colorectal cancer with upconversion luminescent NP-based molecular probes†

Chunyan Liu,<sup>‡a</sup> Yifei Qi,<sup>‡b</sup> Ruirui Qiao,<sup>a</sup> Yi Hou,<sup>a</sup> Kaying Chan,<sup>b</sup> Ziqian Li,<sup>b</sup> Jiayi Huang,<sup>a</sup> Lihong Jing,<sup>a</sup> Jun Du<sup>\*b</sup> and Mingyuan Gao<sup>\*a</sup>

Early detection and diagnosis of cancers is extremely beneficial for improving the survival rate of cancer patients and molecular imaging techniques are believed to be relevant for offering clinical solutions. Towards early cancer detection, we developed a primary animal colorectal cancer model and constructed a tumor-specific imaging probe by using biocompatible NaGdF<sub>4</sub>:Yb,Er@NaGdF<sub>4</sub> upconversion luminescent NPs for establishing a sensitive early tumor imaging method. The primary animal tumor model, which can better mimic the human colorectal cancer, was built upon continual administration of 1,2-dimethylhydrazine in Kunming mice and the tumor development was carefully monitored through histopathological and immunohistochemical analyses to reveal the pathophysiological processes and molecular features of the cancer microenvironment. The upconversion imaging probe was constructed through covalent coupling of PEGylated core-shell NPs with folic acid whose receptor is highly expressed in the primary tumors. Upon 980 nm laser excitation, the primary colorectal tumors in the complex abdominal environment were sensitively imaged owing to the ultralow background of the upconversion luminescence and the high tumor-targeting specificity of the nanoprobe. We believe that the current studies provide a highly effective and potential approach for early colorectal cancer diagnosis and tumor surgical navigation.

Received 9th November 2015,  
Accepted 20th November 2015  
DOI: 10.1039/c5nr07858j

www.rsc.org/nanoscale

## 1. Introduction

Colorectal cancer (CRC) has become one of the leading causes of morbidity and mortality throughout the world.<sup>1</sup> In recent years, the incidence and mortality rates for colorectal cancer have risen gradually, especially in economically developing countries.<sup>2</sup> The survival rate for CRC is highly dependent upon the disease stage at diagnosis. For example, the 5-year survival rate ranges from 90% for CRC at the localized stage, approximately 70% for regional spreading, to less than 10% for distant metastases.<sup>2,3</sup> Although most of the CRCs can be prevented through regular colonoscopy coupled with the removal of polyps, smaller polyps and advanced adenomas are often

missed, leading to an increased risk of tumorigenesis or cancer recurrence.<sup>3</sup> Therefore, the treatment of CRC based on accurate diagnosis at an early stage is crucial for providing more opportunity to raise the survival rate of patients.

Molecular imaging, relying on specific recognition between the imaging probe and receptors in the region of interest, provides an ideal tool for cancer diagnosis through acquiring the anatomical and even molecular information of malignant tumors.<sup>4</sup> Common imaging techniques include X-ray computed tomography (CT), magnetic resonance imaging (MRI), positron emission tomography (PET), single photon emission CT (SPECT), ultrasound, and versatile optical imaging methods,<sup>5–9</sup> among them the rapidly developed optical imaging attracts increasing attention due to its high detection sensitivity and low cost. Dyes, quantum dots (QDs), and other luminescent materials as optical signal vehicles are intensively explored for clinical applications.<sup>10–13</sup> However, the conventional luminescent materials suffer from limitations such as low penetration depth of tissues, high background signals from the autofluorescence of tissues beyond the target, and photobleaching.<sup>9,14</sup> Thus, their applications are not satisfying for *in vivo* imaging of tumors especially those in the complex environment of the abdominal cavity and the digestive tract.

<sup>a</sup>Institute of Chemistry, Chinese Academy of Sciences, Bei Yi Jie 2, Zhong Guan Cun, Beijing 100190, China. E-mail: gaomy@iccas.ac.cn; Fax: +86 10 8261 3214

<sup>b</sup>School of Pharmaceutical Sciences, Sun Yat-sen University, Guangzhou 510006, China. E-mail: dujun@mail.sysu.edu.cn

† Electronic supplementary information (ESI) available: (1) Molecular structure of Jeffamine-modified FA; (2) immunohistochemical analysis of FR expression in the colorectal tissue derived from mice treated with NaCl at different weeks; (3) biodistributions of probes of NP-FA and NP-IgG in the main organs of mice. See DOI: 10.1039/c5nr07858j

‡ These authors contributed equally to this work.

Recently, upconversion luminescent (UCL) rare-earth (RE) nanoparticles (NPs) have been demonstrated to possess enormous potential in tumor imaging detection.<sup>14,15</sup> Owing to the unique properties associated with f-electrons, the UCL NPs exhibit superior optical properties such as large effective Stokes shifts, sharp emissions, long luminescence lifetimes, and high resistance to photobleaching. Furthermore, deeper tissue penetration of the excitation for UCL and lower background noise benefit their *in vivo* imaging applications. Because UCL is typically absent or low in most materials in contrast to fluorescence, the *in vivo* detection of tumors tagged with UCL particles is especially favorable for excluding the strong fluorescence interference of the ingested foods for CRC detection. Our previous work revealed that NaGdF<sub>4</sub>:Yb,Er NPs can successfully be used in the optical imaging of tumors smaller than 2 mm in diameter *via* active targeting.<sup>5</sup> Upon further surface coating, the luminescence efficiency of the resulting NaGdF<sub>4</sub>:Yb,Er@NaGdF<sub>4</sub> NPs could be improved by nearly two orders of magnitude, which enabled the following imaging of lymphatic micrometastasis of 1 mm apart from the metastatic lymph node in an orthotopic mouse model of human gastric cancer.<sup>16</sup> The ultrahigh sensitivity merits the consideration of UCL nanoprobe in early cancer detection and studies. Moreover, the characteristic green emission of Yb, Er-codoped NaGdF<sub>4</sub> is beneficial for visualizing the regions of lesions and thus shows remarkable potential in surgical navigation applications.

The biological features of tumorigenesis are also of great significance for early detection of tumors. Appropriate pre-clinical animal tumor models are essentially required to reproduce the aspects of the tumor microenvironment and emulate a number of important biological features of cancer progression, angiogenesis, metastasis and resistance.<sup>16,17</sup> The tumor model systems available in rodents are often adopted to uncover the disease biology. For example, the mouse subcutaneous tumor model is a common one and easy to establish and monitor, however the subcutaneous milieu cannot replicate the microenvironment of the original anatomic site.<sup>17,18</sup> Different from the other tumor models established by implanting tumor cells or tissues, the primary tumor is built through continual stimulation with chemical carcinogens over a long time period to induce neoplasms occurring spontaneously in the tissue of interest.<sup>19,20</sup> A recent study suggested that models of primary colorectal cancer are morphologically similar to human colon tumors.<sup>20</sup> If the complex pathophysiological processes of carcinogenesis of human colorectal tumors, involving the changes of cellular morphology and the expression of oncomarkers, can be simulated, it will be very helpful for realizing CRC detection and studies.

Herein, we report a primary colorectal tumor model built with Kunming mice using a chemical inducing agent, 1,2-dimethylhydrazine (DMH), to promote DNA hypermethylation of colorectal epithelial cells.<sup>19,20</sup> Histological analysis was carried out to uncover the progression of the colorectal cancer and the expression of the folate receptor (FR). It is known that FR is rarely expressed in normal cells, but overexpressed in various

solid tumors such as breast and ovarian cancers.<sup>23–25</sup> A recent study reveals that FR is also overexpressed in colorectal tumors, which provides a potential target not only for CRC detection, but also for providing staging information and prognostic significance.<sup>26</sup> Based on the positive correlation of FR expression with the cancer progression observed from our animal model, the UCL probes were designed and prepared for the *in vivo* detection of primary colorectal cancers. In brief, the hydrophobic NaGdF<sub>4</sub>:Yb,Er@NaGdF<sub>4</sub> core-shell NPs were synthesized, following our previous investigations on the preparation, biodistribution, and clearance of the RE NPs, as well as *in vivo* tumor imaging,<sup>5,14,16,21,22</sup> and then covalently conjugated with folic acid (FA) after being PEGylated for optical imaging of primary colorectal tumors.

## 2. Results and discussion

### 2.1 Synthesis of core-shell nanoparticles

The preparation of a NaGdF<sub>4</sub>:Yb,Er core and the following growth of a NaGdF<sub>4</sub> shell to achieve NaGdF<sub>4</sub>:Yb,Er@NaGdF<sub>4</sub> core-shell particles were carried out according to the methods described in our previous work.<sup>22</sup> Fig. 1a and b show that the core NPs are spherical with an average size of  $15.9 \pm 0.6$  nm, while they are slightly elongated upon shell growth but showing no change in the uniformity of the particles, indicating that no secondary nucleation occurred during the shell coating process. The average size of the resulting core-shell NPs is  $30.5 \pm 2.0$  nm  $\times$   $22.4 \pm 1.3$  nm. The powder X-ray diffraction (XRD) patterns in Fig. 1c reveal that the core particles are hexagonal nanocrystals and the NaGdF<sub>4</sub> coating did not alter the crystalline phase structure of the core but significantly enhanced the luminescence efficiency by a factor of 134, higher than that achieved previously,<sup>16</sup> which is essential for effectively increasing the sensitivity for the following tumor detection. In fact, the formation of short rod-like nanocrystals was previously observed owing to the slightly superior growth tendency along [001] direction of hexagonal nanocrystals.<sup>5</sup>

### 2.2 Preparation of the tumor imaging probe

The as-prepared core-shell NPs were hydrophobic since they were stabilized with oleic acid (OA). An asymmetric polyethylene glycol (PEG) bearing a maleimide group at one end and a diphosphate group at the other (mal-PEG-dp) was used to replace the OA ligand to render the RE particles biocompatible, based on the fact that the diphosphate group possesses a higher binding affinity than the carboxyl group to Gd<sup>3+</sup>. After PEGylation, the NPs showed excellent colloidal stability both in water and PBS buffer, which is favorable for a prolonged blood half-time and effective tumor targeting after being delivered through intravenous injection.

The structure design of the nanoprobe plays a pivotal role in the sensitivity of tumor detection. FA as a high-affinity ligand for FR was previously used in targeted delivery of nanoprobe to the FR-overexpressed cancers.<sup>27</sup> However, FA (MW = 441.4) has a poor solubility in water. The coupling

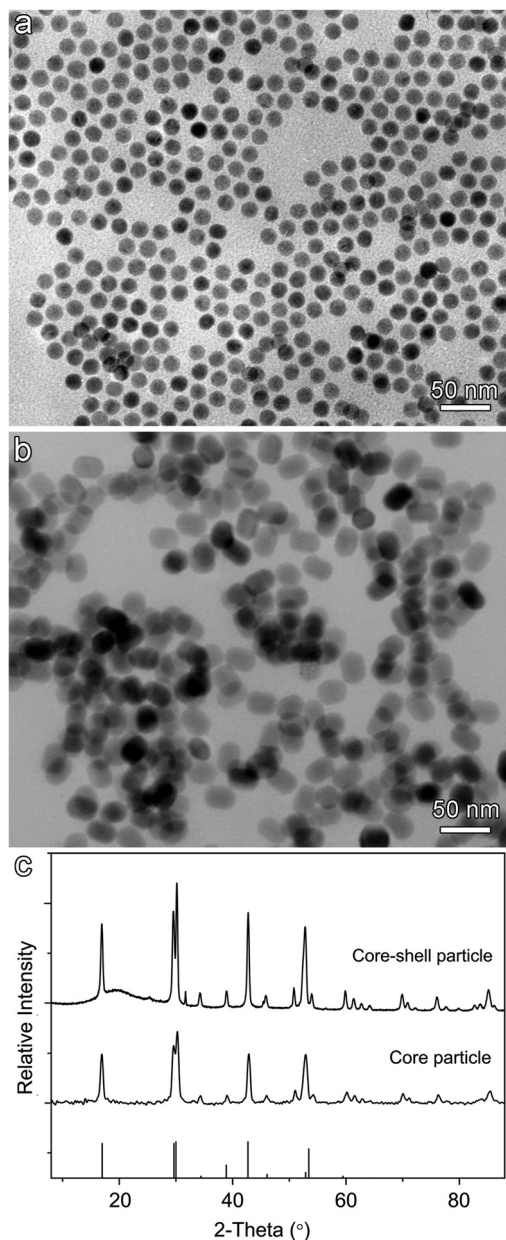


**Fig. 1** TEM images of NaGdF<sub>4</sub>:Yb,Er core NPs (a) and NaGdF<sub>4</sub>:Yb,Er@NaGdF<sub>4</sub> core-shell NPs (b), together with their XRD patterns (c). The scale bars embedded in the TEM images correspond to 50 nm and the vertical line pattern in the bottom frame is the standard XRD data for hexagonal NaGdF<sub>4</sub> according to JCPDS card (No. 27-0699).

reaction with NPs often has to be carried out in a mixture of water and dimethyl sulfoxide (DMSO), and the resulting conjugates need to be transferred into PBS buffer after the reaction. The whole procedure is complicated and the colloidal stability of the resulting NPs labeled with FA is remarkably limited by the number of FA molecules attached due to its strong hydrophobicity. To overcome this drawback, a Jeffamine-modified FA (Fig. S1†) was designed and synthesized. Two Jeffamine molecules were covalently coupled with one FA molecule through one of the amino groups of each Jeffamine molecule

via amidation reaction. The Jeffamine-FA conjugate is very readily dissolved in water showing high solubility. Upon further reaction through the remaining amino group in Jeffamine-FA with the maleimide residues of PEG ligands capped on the particle surface, the NaGdF<sub>4</sub>:Yb,Er@NaGdF<sub>4</sub>-FA conjugates were obtained.

The impact of the above conjugation reaction on the properties of the core-shell NPs was investigated with both conventional electron spectroscopy and dynamic light scattering (DLS). The absorption spectroscopy results, as shown in Fig. 2a, reveal that the overall absorption of the original NPs is greatly enhanced after the conjugation reaction with FA, and meanwhile two absorption peaks appear at around 281 nm

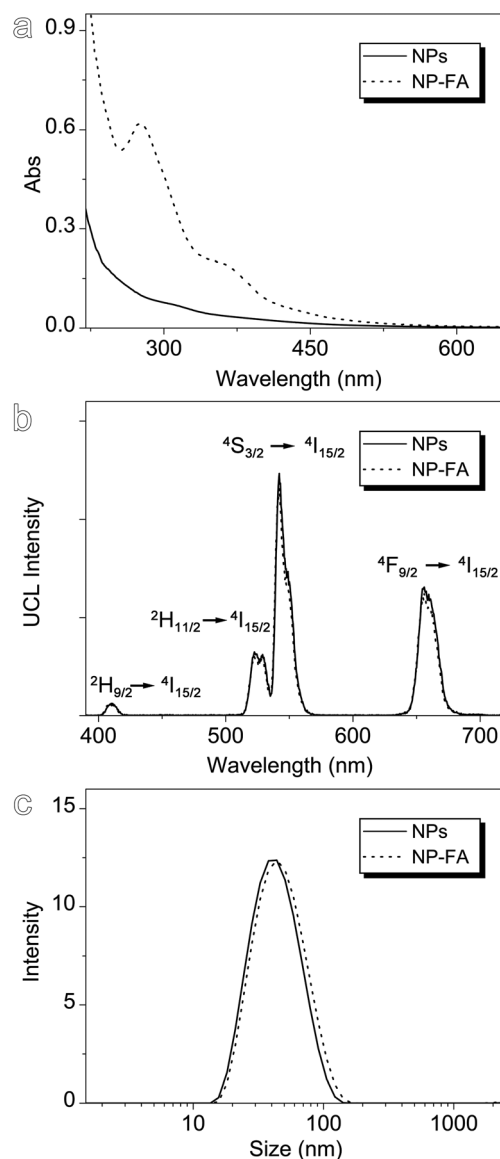


**Fig. 2** Normalized absorption spectra of the core-shell NPs and the NP-FA conjugates (a), normalized upconversion luminescence spectra of NPs and NP-FA in water under 980 nm laser excitation (b), and the hydrodynamic size distribution profiles of NPs and NP-FA (c).

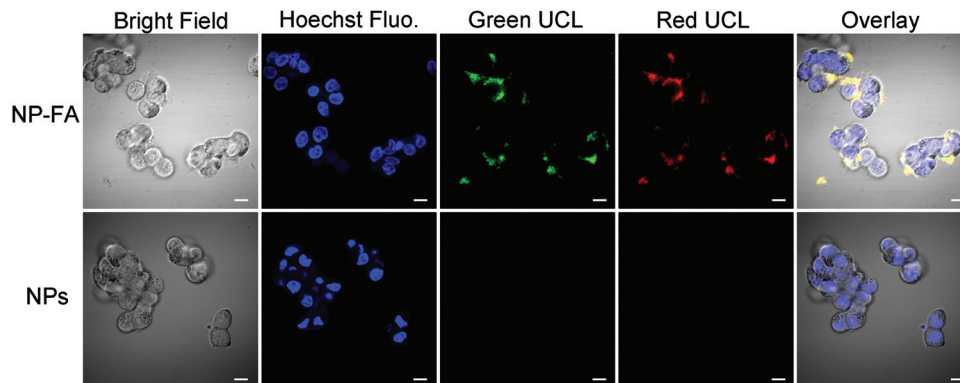


**Fig. 3** Bright field images (Bright Field), fluorescence images (Hoechst Fluor., collected at 420–520 nm for nuclei stained with Hoechst), upconversion luminescence images (Green UCL and Red UCL collected at 500–570 nm and 600–700 nm, respectively) together with merged images (Overlay) of LS180 cells incubated with NP-FA and NPs, respectively. The scale bars correspond to 10  $\mu\text{m}$ .

and 346 nm that are typical absorption bands of FA. To quantitatively characterize the resulting conjugates, the difference between the absorption spectra of NPs and NP-FA solutions containing identical concentration of  $\text{RE}^{3+}$  was carefully extracted. By using the bulk density of  $\text{NaGdF}_4$  for NPs, the number of FA molecules was calculated to be around  $\sim 590$  per NP. Then it is interesting to further reveal the impact of the surface capped FA on the optical properties of NPs. As shown in Fig. 2b, the  $\text{NaGdF}_4\cdot\text{Yb,Er@NaGdF}_4$  NPs exhibit distinct emissions centered at 409, 521, 541, and 655 nm which correspond to the transitions from  $^2\text{H}_{9/2}$ ,  $^2\text{H}_{11/2}$ ,  $^4\text{S}_{3/2}$ , and  $^4\text{F}_{9/2}$  states to the  $^4\text{I}_{15/2}$  state of  $\text{Er}^{3+}$ , respectively. The NP-FA conjugates present nearly identical emission features, suggesting that the conjugation reactions did not alter the optical properties of NPs. The following DLS results in Fig. 2c reveal that the intensity-weighted hydrodynamic size of NPs is increased from 40.2 nm to 43.5 nm after the conjugation reaction. The size difference in consequence of the conjugation reaction is less evident in comparison with that often observed from larger conjugating molecules such as IgG.<sup>28</sup> This is because the FA molecule is on the one hand much smaller than IgG, and on the other hand less solvated due to its hydrophobic structure. However, the light scattering profile remains nearly unchanged through the conjugation reaction except for the shift owing to the increased size of NP-FA conjugates, suggesting that the coupling reaction did not lead to unwanted aggregates even though the FA moieties are hydrophobic.

To validate the targeting ability of the NP-FA probes, LS180 cells, on the surface of which FR is highly expressed, were used for *in vitro* cellular experiments. As displayed in Fig. 3, the cells co-incubated with the NP-FA probes show intense UCL signals at 500–570 nm (green channel) and 600–700 nm (red channel) under 980 nm laser excitation. The overlay of bright-field images, nuclei images upon staining with Hoechst, and the UCL images of cells reveals that the nanoprobe is predominantly located at the cell membrane. In contrast, no upconversion signal is presented by the cells incubated with the mother

NPs. These results demonstrate that the NP-FA probe possesses outstanding binding affinity to the target cells.

### 2.3 Establishment of the primary colorectal tumor model

The primary tumor model was constructed on Kunming mice by continual subcutaneous administration of DMH for more than 25 weeks, and the mice treated with NaCl solution was set as the control group. Histopathological and immunohistochemical (IHC) analyses were carried out to follow the progression stages of the neoplasm lesions and the expression level of FR at different time points. Hematoxylin and eosin (H&E) staining of the colorectum tissues allows one to distinguish tumor stages over time according to the different degree of gland disorder, lymphoid hyperplasia and infiltration that appeared in the process of colorectal carcinoma. The histopathological results, as shown in the left column of Fig. 4, reveal that aberrant crypt and lymphoid hyperplasia start to appear on the 13th and 15th week, respectively, followed by microadenoma on the 17th week, and adenoma on the 21st week. Meanwhile, IHC staining analysis was carried out to monitor the FR expression in the colorectum tissues. The tissues stained with anti-FR exhibit an obvious brown color around the glands throughout the whole period from the 13th to the 21st week (right column of Fig. 4), in huge contrast to the tissues treated with PBS (middle column of Fig. 4), which clearly demonstrates that the expression level of FR is elevated over time. Careful observations reveal that the degree of the brown color of single stained glands is nearly unchanged at different progressing stages, but the number of brown sites significantly increased in extensive histological sections. Whilst no apparent FR staining was observed in the colorectum tissues collected from the mice receiving continual injection of NaCl solution (shown in Fig. S2<sup>†</sup>). These results suggest that DMH can effectively stimulate the transformation of benign colorectal tissue to malignant tissue. Previous studies suggest that DMH carcinogenesis is closely related to DNA hypermethylation of the colorectal epithelial cells,<sup>19,20,29</sup>

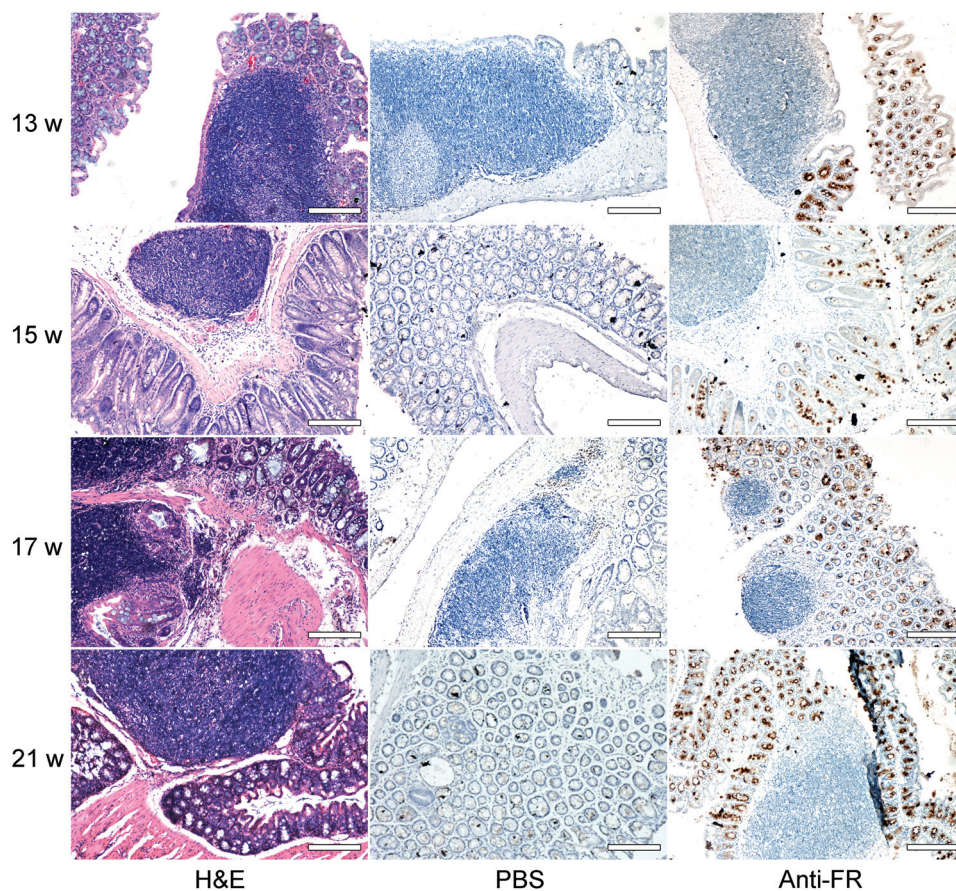


**Fig. 4** Microscopic images of colorectum tissues of mice treated with DMH at different time points for H&E staining images (left), immunohistochemical staining after being treated with PBS (middle) and anti-FR (right), respectively. The scale bars correspond to 200 μm.

and DNA methylation is closely related to the abnormal expression of FR irrespective of the DMH stimulation.<sup>23</sup> Well in accordance with these findings, the above results strongly suggest that the abnormally expressed FR may potentially be used as a target for colorectal tumor staging. Although the above experiments for the first time disclosed a detailed morphological evolution of colorectum tissues towards malignant tumors, accompanied by over-expression of FR, the adenoma remains a precancerous (pre-malignant) lesion. Along with further increased expression, as shown below, FR may become a relevant target in primary colorectal tumors.

#### 2.4 UCL imaging of the primary colorectal tumors

*In vivo* UCL imaging was performed with randomly chosen mice out of a group obtained on the 25th week of DMH treatment, with the rest of them being used for evaluating the carcinoma transformation and FR expression. The NP-FA probe was intravenously injected, and the conjugate of NPs with IgG (NP-IgG) was used as a control. The reference probe was prepared according to a previously reported protocol.<sup>21</sup> The intestine is long and flexural, and covered by a thick adipose layer of the abdomen, therefore a surgery was performed under

anaesthesia right before the imaging measurements that were typically carried out 6 h after the injection of the conjugates and this imaging time point was carefully chosen according to our previous studies.<sup>5,21</sup>

As shown in Fig. 5, an identifiable luminescence signal is clearly presented in the colorectum region 6 h post injection with a signal-to-noise ratio (SNR) up to 6.3, calculated with  $(I_s - I_b)/(I_n - I_b)$  ( $I_s$ : signal intensity;  $I_b$ : background intensity;  $I_n$ : noise intensity). Furthermore, under 980 nm laser excitation the surrounding tissue and the digested feed don't show any luminescence signal, which manifests the charm of UCL imaging in comparison with conventional down-conversion luminescence imaging. Because in the latter case ultra-violet-visible (UV) excitation induces strong interference from both the autofluorescence of the surrounding tissues and the fluorescence of the digested foods apart from its low penetration depth. Most importantly, almost no observable signal is generated by the control probe. Following the imaging experiments, the main organs such as the liver, spleen, kidneys, lungs, and small intestines were harvested for determining the biodistribution of both the probes by measuring the Gd contents. As shown in Fig. S3,† the liver and spleen

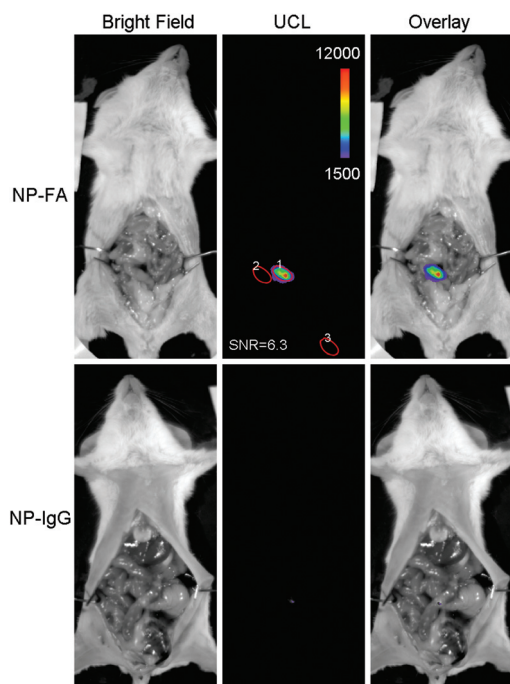


**Fig. 5** Bright field images (left), color-coded UCL images (middle), and the merged images (right) captured 6 h after intravenous injection of NP-FA (top) and NP-IgG (bottom), respectively. The regions of interest are encircled with red lines and labeled by 1 ( $I_s$ ), 2 ( $I_n$ ), 3 ( $I_b$ ), respectively, for determining SNR.

uptake is dominant for both the probes, which is typical for nanoprobe owing to the fact that the immune system tends to purify the blood of foreign particles. It deserves to be mentioned that the experimental results shown in Fig. 5 are just representative data out of three independent imaging experiments. Moreover, no upconversion signal is shown from the liver simply because the excitation light beam (2 cm in diameter) did not cover the liver region.

### 2.5 Histological studies of the primary colorectal tumor

To further confirm that the UCL signal is from the colorectal tumor, the luminescent tissue was harvested under the guidance of UCL light for histopathological analysis upon H&E and IHC staining. Two adjacent slices of the tissue were carefully chosen for showing the malignancy of the tissue and FR expression. As shown in Fig. 6a and b, the morphological characteristics of the original colorectal glands have been completely lost, and clear carcinogenesis can be confirmed from the morphology change of the cells in the enlarged image in Fig. 6b. Moreover, the invasive front of carcinomas is limited to the submucosal layer, away from the muscular layers. Generally, following the formation of carcinoma, there are five distinct stages for differentiating the tumor development, *i.e.*, stage 0: the tumor locates in the mucosal layer of colon; stage I: the invasion front reaches the muscularis layer; stage II: the tumor perforates the serosa; stage III: the surrounding lymph nodes are involved; stage IV: distal metastasis occurs.<sup>30</sup> There-

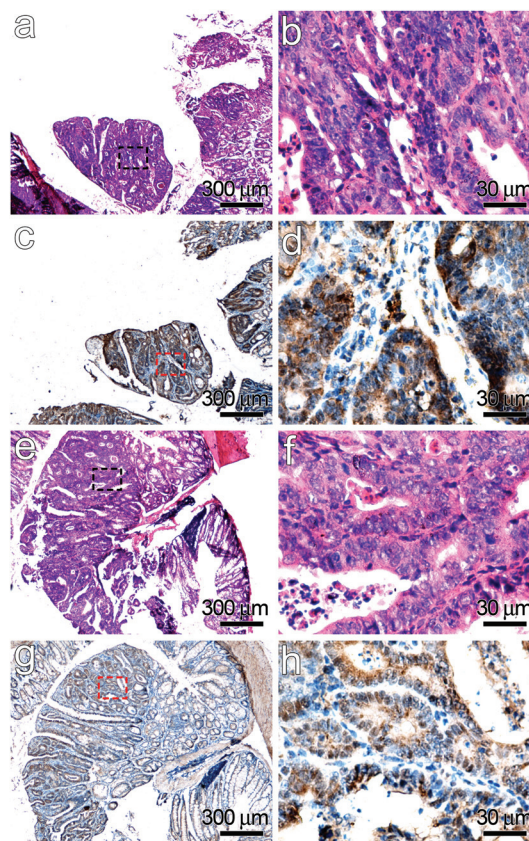


**Fig. 6** Histopathological images (a and b) and IHC analysis of FR (c and d) of adjacent slices of the luminescent tissue from the mice after intravenous injection of NP-FA as well as those of the control group of NP-IgG (e–h). Part of the malignant lesion highlighted by dashed lines is enlarged to better show the carcinoma cell characteristics and the staining of FR respectively. The scale bars for a, c, e, g correspond to 300  $\mu\text{m}$ , and b, d, f, h correspond to 30  $\mu\text{m}$ .

fore, the above histopathological staining results suggest that the UCL signal comes from an early stage CRC, which is further confirmed by the following immunohistochemical staining studies.

As shown in Fig. 6c and d, the slice adjacent to that in Fig. 6a and b presents a very heavy brown color, displaying a higher level of FR expression in comparison with those shown in Fig. 4. Careful observations suggest that the brown color is thickened due to heavy staining of the cancer cells. The histological results strongly support the FA-mediated cancer targeting strategy for the NP-FA probe, because similar histopathological and IHC staining results were also observed from the control group as shown in Fig. 6e–h, but the NP-IgG control probe did not give rise to an observable signal. Although the NP-FA probe has successfully been used for imaging 0 stage colorectal cancer as discussed above, the results shown in Fig. 4 and 6 suggest that it may also be possible to image precancerous cancers if the sensitivity of the nanoprobe is further improved.

### 3. Conclusion

In summary, a primary mice colorectal cancer model was successfully established through a chemical inducing approach and systematic histopathological and immunohistochemical studies revealed that the malignant development of colorectal carcinoma was accompanied by the abnormal expression of FR. FA was therefore covalently attached to the surface of biocompatible NaGdF<sub>4</sub>:Yb,Er@NaGdF<sub>4</sub> UCL NPs for colorectal cancer detection. The *in vivo* UCL imaging demonstrated that the NP-FA probe well enabled the visualization of colorectal tumors at 0 stage under 980 nm laser excitation and the following histopathological and immunohistochemical assays strongly suggested that the FA/FR recognition was responsible for the colorectal cancer-specific imaging. In conclusion, the current studies not only provide detailed molecular information on the occurrence and evolution of colorectal cancer, but may also provide a potential approach for detecting tumors in the complex body environment upon integration with endoscopy.

### 4. Experimental section

#### 4.1 Chemicals

GdCl<sub>3</sub>·6H<sub>2</sub>O, YbCl<sub>3</sub>·6H<sub>2</sub>O, ErCl<sub>3</sub>·6H<sub>2</sub>O, OA, 1-octadecene (ODE), ammonium fluoride, FA, pentobarbital sodium, 2-iminothiolane hydrochloride, tris(2-carboxyethyl) phosphine hydrochloride (TCEP), murine immunoglobulin G (IgG), and DMH were purchased from Sigma-Aldrich. mal-PEG-dp and Jeffamine modified FA were customized products provided by Beijing Oneder Hightech Co. Ltd. Human colorectal cancer cell line LS180 was obtained from the Oncology School of Peking University. DMEM high glucose (HyClone), F-12K Nutrient Mixture (Gibco), fetal bovine serum (HyClone), penicillin, and streptomycin were bought from Beijing Biodee Biotechnology Co. Ltd. The SP reagent kit, biotinylated anti-rabbit secondary antibody, streptavidin-horseradish peroxidase complex, and the diaminobenzidine kit were bought from Zhongshan Goldenbridge Biotechnology Company. Other analytical grade chemicals such as sodium bicarbonate, ethanol, cyclohexane, DMSO and tetrahydrofuran (THF) were bought from Sinopharm Chemical Reagent Beijing, Co., Ltd.

#### 4.2 Synthesis of upconversion NPs

The synthesis of the NaGdF<sub>4</sub>:Yb,Er NPs was through a replacement reaction at high temperature, and the NaGdF<sub>4</sub>:Yb,Er@NaGdF<sub>4</sub> core-shell NPs was obtained *via* a seed-mediated method according to our previous procedure.<sup>22</sup> Typically, GdCl<sub>3</sub>·6H<sub>2</sub>O (0.80 mmol), YbCl<sub>3</sub>·6H<sub>2</sub>O (0.18 mmol), and ErCl<sub>3</sub>·6H<sub>2</sub>O (0.02 mmol) were mixed with 14 mL OA and 16 mL ODE in a 100 mL flask. After forming a homogeneous solution under nitrogen protection by heating to 150 °C, the solution was cooled down to 50 °C and 10 mL of a methanol solution with NaOH (2.5 mmol) and NH<sub>4</sub>F (3.6 mmol) was added drop-

wise. After stirring at this temperature for 30 min, the methanol in the system was removed under vacuum at 100 °C. Subsequently, the reaction mixture was heated to 300 °C under atmospheric pressure for 1 h. The resultant nanoparticles were precipitated by ethanol, collected by centrifugation, re-dispersed in THF, and washed with ethanol for three cycles. The subsequent deposition of the NaGdF<sub>4</sub> shell followed a similar process of the preparation of NaGdF<sub>4</sub>:Yb,Er core particles. Briefly, 0.33 mmol core particles dispersed in THF and 1 mmol GdCl<sub>3</sub>·6H<sub>2</sub>O were added to a 100 mL three-neck round-bottom flask containing 4 mL OA and 16 mL ODE. The growth of the NaGdF<sub>4</sub> shell and the following purification procedures for the core@shell particles were the same as those for the core nanocrystals.

#### 4.3 Preparation of water-soluble NPs and nanoprobe

The PEGylation of NaGdF<sub>4</sub>:Yb,Er@NaGdF<sub>4</sub> NPs was achieved *via* ligand exchange following our previously reported protocol.<sup>21</sup> Then, Jeffamine modified FA was conjugated to the core-shell NPs *via* “click” reaction. In detail, approximately 0.5 mg Jeffamine-modified FA was mixed with 0.2 mg 2-iminothiolane hydrochloride in 1 mL water, and the reaction mixture was kept for 2 hours at room temperature. Then, 6 mg PEGylated NPs were added into the above solution and the conjugation reaction was allowed for 30 min. The resulting NP-FA conjugates were purified by 30k MWCO centrifugal devices to remove the unreacted Jeffamine-FA and then transferred into 1× PBS buffer, and stored at 4 °C for further use.

The NP-IgG conjugates were prepared according to our previous publications.<sup>21</sup> Typically, IgG (1 mg mL<sup>-1</sup> in 10× PBS) was subjected to mild reduction by TCEP to convert the disulfide groups in the Fc fragments to thiol groups. Then, the partially reduced IgG was purified by using 30k MWCO centrifugal devices. The (mal-PEG-dp)-coated core@shell NPs in tris-buffered saline (pH 7.04) were added to the partially reduced IgG solution and the reaction was kept for 30 min. After purifying by ultrafiltration, the conjugate was redispersed in 1× PBS buffer for further use.

#### 4.4 Characterization of NPs and nanoprobe

TEM images of the NPs were obtained using a JEM-100CXII electron microscope at an acceleration voltage of 100 kV. The particle size was determined by counting at least 300 nanocrystals per sample. The XRD patterns of the particle samples were recorded on a Regaku D/Max-2500 diffractometer under Cu Kα<sub>1</sub> radiation ( $\lambda = 1.54056 \text{ \AA}$ ). The concentration of Gd<sup>3+</sup> was determined by using an inductively coupled plasma atomic emission spectrometer (ICP 5300DV). The absorption spectra were recorded at room temperature on a Cary 50 UV-Vis spectrophotometer. The UCL spectra were recorded on a Cary Eclipse fluorescence spectrophotometer equipped with a 980 nm CW laser diode (2 W) serving as the excitation source. DLS measurements were carried out at 298.0 K with Nano ZS (Malvern) equipped with a solid state He-Ne laser ( $\lambda = 632.8 \text{ nm}$ ) for determining the hydrodynamic profiles of the

core-shell NPs and monitoring the following bioconjugation reactions.

#### 4.5 Cell culture and *in vitro* cellular imaging

Human colorectal cancer cell line LS180 was cultured in a medium of DMEM high glucose and F-12K Nutrient Mixture (1 : 1) supplemented with 10% fetal bovine serum, 100 U mL<sup>-1</sup> penicillin, and 0.1 mg mL<sup>-1</sup> streptomycin at 37 °C under a 5% CO<sub>2</sub> atmosphere.

Approximately 10<sup>6</sup> LS180 cells were seeded in the wells of two confocal capsules and incubated overnight at 37 °C under 5% CO<sub>2</sub> to allow a firm adherence. After being rinsed with PBS buffer, the cells were incubated with the NP-FA probe and the NPs, respectively, for 6 h at 37 °C. After that, the cells were rinsed three times with PBS to remove the unbound particles. The cells were further incubated with 5 μg mL<sup>-1</sup> Hoechst 33258 for nuclei staining. The imaging of cells was carried out on a confocal microscope (Olympus FV 1200) equipped with an extra 980 nm laser. The luminescence signals of the cells were detected in two channels: the green channel (500–570 nm) and the red channel (600–700 nm). For the nuclei imaging, the excitation line was tuned to 405 nm and the fluorescence signals were collected in a range of 420–520 nm.

#### 4.6 Establishment of the primary colorectal tumor model

The primary colorectal tumor models used were established upon continual administration of DMH in female Kunming mice (4–6 weeks). The mice were divided into two groups randomly. One group ( $n = 35$ ) was given subcutaneous injections of DMH dissolved in normal saline and neutralized with sodium bicarbonate (pH = 7.0) weekly at a dose of 35 mg per kg body weight for 25 weeks, and the other group ( $n = 12$ ) injected with the same concentration NaCl solution was set as the control. The mice were sacrificed for the investigation of the tissue morphology and the FR expression level in the region of colorectum on the 13th, 15th, 17th, 21st, and 25th weeks, respectively, post injection.

#### 4.7 UCL imaging of primary colorectal tumors

The *in vivo* imaging experiments were carried out on the 25th week after the first shot of the chemical carcinoma inducing agent. The dose level of the nanoprobe for imaging was 15 mg of Gd per kilogram body weight. The mice were anesthetized with 1% pentobarbital sodium prior to the surgical manipulation, typically 6 h after the intravenous injection of the nanoprobe. The UCL images of tumors were captured using a Berthold LB 983 *in vivo* imaging system with an external 0–20 W adjustable laser. Excitation was provided by the CW infrared laser at 980 nm and UCL signals were collected by electron multiplying charge coupled devices (EMCCD) equipped with an 460–690 nm bandpass filter. After imaging, the mice were executed, and the main organs were harvested. The uptake of NP-FA and NP-IgG probes by the organs was determined with ICP-AES after they were eroded by concentrated HNO<sub>3</sub> and H<sub>2</sub>O<sub>2</sub>.

All animal procedures were in agreement with the guidelines of Sun Yat-sen University Institutional Animal Care and Use Committee.

#### 4.8 Histological study

In brief, formalin-fixed and paraffin-embedded colorectum tissue sections of 5 μm were first deparaffinized and hydrated. High-pressure antigen retrieval was performed using citrate buffer (pH = 6.0). Endogenous peroxidase was quenched with 3% hydrogen peroxide in methanol for 15 min, followed by incubation with normal serum to block non-specific staining. Rabbit anti-FR was then incubated with the sections overnight at 4 °C; after washing, the tissue sections were treated with the biotinylated anti-rabbit secondary antibody, followed by further incubation with the streptavidin-horseradish peroxidase complex. After staining with the diaminobenzidine kit (DAB), the sections were counterstained with hematoxylin. A negative control was performed simultaneously, and PBS was used instead of the primary antibody of rabbit anti-FR.

After the optical imaging, the luminescent regions were harvested under the guidance of luminescence, and then kept in 10% formalin for 3 days. After being embedded into paraffin, the fixed tissues were sliced. Part of the slices was stained with hematoxylin and eosin, and part of the slices was subjected to FR staining, and then the stained tissues were subjected to microscopy study.

## Acknowledgements

This work was financially supported by the National Basic Research Program of China (2011CB935800), NSFC (21403250, 21203211, 81471726, 21321063), and CAS (CMS-PY-201309, CMS-PY-201314).

## References

- 1 A. Jemal, F. Bray, M. M. Center, J. Ferlay, E. Ward and D. Forman, *CA Cancer J. Clin.*, 2011, **61**, 69–90.
- 2 F. A. Hagggar and R. P. Boushey, *Clin. Colon Rectal Surg.*, 2009, **22**, 191.
- 3 J. M. Richter, E. J. Campbell and D. C. Chung, *Clin. Colorectal Cancer*, 2014, **14**, 46–51.
- 4 R. Weissleder, *Science*, 2006, **312**, 1168–1171.
- 5 C. Y. Liu, Z. Y. Gao, J. F. Zeng, Y. Hou, F. Fang, Y. L. Li, R. R. Qiao, L. Shen, H. Lei, W. S. Yang and M. Y. Gao, *ACS Nano*, 2013, **7**, 7227–7240.
- 6 H. Herzog, *Zeitschrift für Medizinische Physik*, 2012, **22**, 281–298.
- 7 E. C. Cho, C. Glaus, J. Chen, M. J. Welch and Y. Xia, *Trends Mol. Med.*, 2010, **16**, 561–573.
- 8 H. Chen, Z. Zhen, T. Todd, P. K. Chu and J. Xie, *Mat. Sci. Eng. R-Rep.*, 2013, **74**, 35–69.
- 9 C. Bouzigues, T. Gacoin and A. Alexandrou, *ACS Nano*, 2011, **5**, 8488–8505.

- 10 R. J. Byers and E. R. Hitchman, *Prog. Histochem. Cytochem.*, 2011, **45**, 201–237.
- 11 J. H. Lee, Y. W. Jun, S. I. Yeon, J. S. Shin and J. Cheon, *Angew. Chem., Int. Ed.*, 2006, **45**, 8160–8162.
- 12 K. Ding, L. H. Jing, C. Y. Liu, Y. Hou and M. Y. Gao, *Biomaterials*, 2014, **35**, 1608–1617.
- 13 Y. Hou, J. Zhou, Z. Y. Gao, X. Y. Sun, C. Y. Liu, D. H. Shangguan, W. S. Yang and M. Y. Gao, *ACS Nano*, 2015, **9**, 3199–3205.
- 14 C. Y. Liu, Y. Hou and M. Y. Gao, *Adv. Mater.*, 2014, **26**, 6922–6932.
- 15 D. K. Chatterjee, M. K. Gnanasammandhan and Y. Zhang, *Small*, 2010, **6**, 2781–2795.
- 16 R. R. Qiao, C. H. Liu, M. H. Liu, H. Hu, C. Y. Liu, Y. Hou, K. C. Wu, Y. N. Lin, J. M. Liang and M. Y. Gao, *ACS Nano*, 2015, **9**, 2120–2129.
- 17 M. Loi, D. Di Paolo, P. Becherini, A. Zorzoli, P. Perri, R. Carosio, M. Cilli, D. Ribatti, C. Brignole, G. Pagnan, M. Ponzoni and F. Pastorino, *Int. J. Dev. Biol.*, 2011, **55**, 547–555.
- 18 W. Tseng, X. Leong and E. Engleman, *J. Visualized Exp.*, 2007, 484–484.
- 19 K. M. Pozharisski, Y. M. Kapustin, A. J. Likhachev and J. D. Shaposhnikov, *Int. J. Cancer*, 1975, **15**, 673–683.
- 20 M. J. Jucá, B. C. Bandeira, D. S. Carvalho and A. T. Leal, *J. Coloproctol.*, 2014, **34**, 167–173.
- 21 Y. Hou, R. R. Qiao, F. Fang, X. X. Wang, C. Y. Dong, K. Liu, C. Y. Liu, Z. F. Liu, H. Lei, F. Wang and M. Y. Gao, *ACS Nano*, 2013, **7**, 330–338.
- 22 C. Y. Liu, W. Ma, Z. Y. Gao, J. Y. Huang, Y. Hou, C. L. Xu, W. S. Yang and M. Y. Gao, *J. Mater. Chem. C*, 2014, **2**, 9637–9642.
- 23 L. C. Hartmann, G. L. Keeney, W. L. Lingle, T. J. H. Christianson, B. Varghese, D. Hillman, A. L. Oberg and P. S. Low, *Int. J. Cancer*, 2007, **121**, 938–942.
- 24 J. Barar, V. Kafil, M. H. Majd, A. Barzegari, S. Khani, M. Johari-Ahar, D. Asgari, G. Coukos and Y. Omid, *J. Nanobiotechnol.*, 2015, 13.
- 25 G. Toffoli, C. Cernigoi, A. Russo, A. Gallo, M. Bagnoli and M. Boiocchi, *Int. J. Cancer*, 1997, **74**, 193–198.
- 26 J. Shia, D. S. Klimstra, J. R. Nitzkorski, P. S. Low, M. Gonen, R. Landmann, M. R. Weiser, W. A. Franklin, F. G. Prendergast, L. Murphy, L. H. Tang, L. Temple, J. G. Guillem, W. D. Wong and P. B. Paty, *Hum. Pathol.*, 2008, **39**, 498–505.
- 27 L. Q. Xiong, Z. G. Chen, M. X. Yu, F. Y. Li, C. Liu and C. H. Huang, *Biomaterials*, 2009, **30**, 5592–5600.
- 28 C. Y. Liu, Q. J. Jia, C. H. Yang, R. R. Qiao, L. H. Jing, L. B. Wang, C. L. Xu and M. Y. Gao, *Anal. Chem.*, 2011, **83**, 6778–6784.
- 29 C. Colussi, S. Fiumicino, A. Giuliani, S. Rosini, P. Musiani, C. Macri, C. S. Potten, M. Crescenzi and M. Bignami, *JNCI, J. Natl. Cancer Inst.*, 2001, **93**, 1534–1540.
- 30 F. Sandouk, F. Al Jerf and A. H. D. B. Al-Halabi, *Gastroent. Res. Pract.*, 2013, 457901.